Available online at www.sciencedirect.com
ScienceDirect
Journal of Nuclear Materials 363–365 (2007) 1011–1015
journal of nuclear materials
www.elsevier.com/locate/jnucmat

Melt damage simulation of W-macrobrush and divertor gaps after multiple transient events in ITER

B.N. Bazylev [a,*], G. Janeschitz [b], I.S. Landman [a], A. Loarte [c], S.E. Pestchanyi [a]

[a] Forschungszentrum Karlsruhe, IHM, P.O. Box 3640, 76021 Karlsruhe, Germany
[b] Forschungszentrum Karlsruhe, Fusion, P.O. Box 3640, 76021 Karlsruhe, Germany
[c] EFDA–CSU, Max-Planck-Institut für Plasmaphysik, D-85748 Garching, Germany

Abstract

Tungsten in the form of macrobrush structure is foreseen as one of two candidate materials for the ITER divertor and dome. In ITER, even for moderate and weak ELMs when a thin shielding layer does not protect the armour surface from the dumped plasma, the main mechanisms of metallic target damage remain surface melting and melt motion erosion, which determines the lifetime of the plasma facing components. The melt erosion of W-macrobrush targets with different geometry of brush surface under the heat loads caused by weak ELMs is numerically investigated using the modified code MEMOS. The optimal angle of brush surface inclination that provides a minimum of surface roughness is estimated for given inclination angles of impacting plasma stream and given parameters of the macrobrush target. For multiple disruptions the damage of the dome gaps and the gaps between divertor cassettes caused by the radiation impact is estimated.

PACS: 52.40.Hf

Keywords: Divertor; Tungsten; Erosion; Heat deposition; ELM; Castelation

1. Introduction

Operation of ITER at high fusion gain is assumed to be the H-mode [1]. A characteristic feature of this regime is the transient release of energy from the confined plasma onto plasma facing components (PFCs) by multiple ELMs (about 10^4 ELMs per ITER discharge), which can play a determining role in the erosion rate and lifetime of these components. Similarly, the transient power fluxes during disruptions can affect significantly their lifetime also. The expected fluxes on the ITER divertor during transients are: Type I ELM energy fluxes of 0.5–4 MJ/m^2 in timescales of 300–600 μs, and thermal quench energy fluxes of 2–13 MJ/m^2 in timescales of 1–3 ms and even higher up to 30 MJ/m^2 in timescale of 10 ms.

Tungsten in form of macrobrush structure is foreseen as one of two candidate materials for the ITER divertor and dome. During intense transient events (TE) in ITER the heat loads at the divertor armour may result in a surface melting and its evaporation [2–4]. Melt motion in the thin layer may

* Corresponding author. Fax: +49 7247824874.
E-mail address: bazylev@ihm.fzk.de (B.N. Bazylev).

0022-3115/$ - see front matter © 2007 Elsevier B.V. All rights reserved.
doi:10.1016/j.jnucmat.2007.01.157

produce surface roughness [2] and droplet splashing [5]. In case of the Type I ELMs and the disruptions when a developed ionized vapor shield protects the surface from the hot plasma, the melting and the melt motion are mainly caused by the radiation from the plasma shield and the gradient of the shield plasma pressure. This shielding layer formed above the divertor surface is a source of intense radiation of GW/m^2 level with durations up to 1 ms for ELMs and up to 15 ms for the disruptions. The intense radiation exposes also the surface of the dome elements nearby and the gaps between divertor cassettes, which may cause their melting, evaporation, and formation of own plasma shield [3,6] thus yielding additional damage.

For the multiple TE the separatrix strike position (SSP) at the divertor plate can vary from one transient event to another one, which may lead to a noticeable decrease of the total damage of the tungsten armour [6]. In ITER even for moderate and weak ELMs, where a weak shielding layer does not protect the armour surface from the dumped plasma, the main mechanisms of metallic armour damage remain surface melting and melt motion erosion caused by direct action of damping plasma at the target surface. An initial assessment of the damage to the macrobrush structure under typical Type I ELM heat loads has been carried out using modified code MEMOS–1.5D [7]. It was shown that fine details of macrobrush structure may play a major role in determination of damage profile: the magnitude of total erosion depends on target design and such parameters of the impacting plasma as the inclination angle and the dynamical plasma pressure ρv^2 (ρ the plasma density and v the plasma velocity).

The radiation near the surface is practically isotropic therefore target design is not as important as it is in case of weak ELMs, however excepting the gaps where the radiation may also produce rather large damage. The erosion of the gaps between macrobrush elements and the gaps between divertor cassettes underwent strong transient loads should be estimated in order to find appropriate solutions for their shape, which may substantially reduce material damage of the gap surfaces. An initial assessment of the gap damage caused by strong TE was carried out using modified code MEMOS–1.5D [8].

In this study the numerical simulations, aiming optimization of such details of the reference ITER macrobrush target design as the angle of the flat macrobrush top surface in respect to the force lines of the applied magnetic field and the gap width, was carried out. Results of numerical simulations of the melt motion erosion for tungsten dome elements facing the divertor plate, the gaps between the cassettes and after repetitive radiation heat loads caused by multiple disruptions with the energy deposition Q of 10–30 MJ/m^2 and the duration τ of 1–10 ms are presented. It is to be noted that corresponding simulations for ELMs have revealed that the heat loads in the range of $Q = 1$–4 MJ/m^2 and $\tau = 0.2$–0.5 ms do not cause any erosion of the dome elements. For different single disruptions and ELMs, the heat loads at the divertor surface are calculated using the two-dimensional MHD code FOREV-2D [9]. The target melt motion erosion is calculated by the fluid dynamics code MEMOS-1.5D (described in Ref. [2]) in the 'shallow water' approximation, with the surface tension and viscosity of molten metal taking into account plasma pressure gradient along the divertor plate, as well as the gradient of surface tension and tangential friction force of the dumping plasma.

2. W-macrobrush optimization simulations

The cross-section of macrobrush armour considered in the numerical simulations on macrobrush optimization is schematically shown in Fig. 1 with typical sizes of the macrobrush elements being the following: diameter of brushes $D = 1$ cm, the depth of the gaps between the brushes h of 1 cm, the width of the gaps 1 mm; the radius of the edge arc 0.5 mm. To find a configuration which provides sufficient gap shadowing and simultaneously prevents top surface overheating, it is assumed that the top surfaces of macrobrush elements have some inclination angle β, so that the upstream brush edge of the neighbor

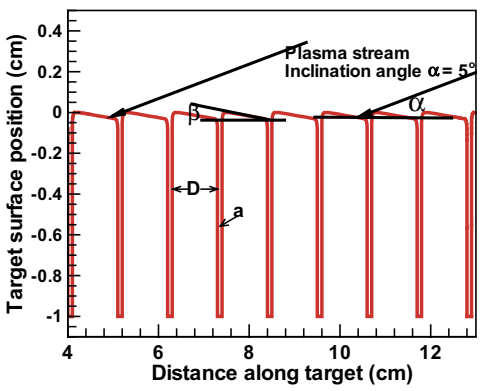

Fig. 1. Sketch of plasma stream interaction with the macrobrush elements.

element shadows the gaps. Optimal angle β may depend on the inclination angle α of the damping plasma and also on the gap width, a. To determine the range for the angle β in which minimal surface roughness of the macrobrush elements is provided, corresponding numerical simulations are performed with the code MEMOS. The heat load parameters for the modified geometry are calculated in accordance with the expressions given in Ref. [7], however taking into account this additional inclination.

It is assumed, that the weak ELM (of 8 cm width and duration $\Delta t = 0.5$ ms) dumps at the W-macrobrush armor with heat load linearly dropping from $Q = 2.1$ MJ/m^2 up to $Q = 0.6$ MJ/m^2 along the target surface (see Fig. 2). Due to a finite Mach number in the plasma stream the actual angles of ion impact can significantly differ from the averaged angle of the plasma impact. Therefore in the calculations of the damage two variants of the plasma impact angles $\alpha = 5°$ and $\alpha = 3°$ are analyzed in order to produce examples of expected effects. For each scenario with given angle of the plasma impact different variants of brush surface inclination angle β are simulated.

The damping plasma heats mainly top surfaces of the brushes and only for scenarios with not sufficient shadowing, the circular edges are also partially heated. The surface temperatures at the top-brush sections depend on the angle β. For all scenarios the maximum thickness of melt layer does not exceed 60 μm. For relatively large inclination angles β, surface temperature in the heated region may rise up to boiling temperature. In the case with not sufficient shadowing, the surface temperature at the upper part of circular surfaces faced to the plasma stream may significantly exceed the average surface temperatures of top-brush segments and intensive evaporation may occur. Due to shadowing, the surface temperature of the lateral brush segments is much below the melting temperature. Such significantly inhomogeneous profile of the surface temperature results also in a large gradient of the surface tension, which significantly intensifies the melt motion. The tangential friction force and the gradient of surface tension produce the melt motion with the melt velocity ranging from 0.2 m/s up to 0.5 m/s along the top-brush sections in the direction of plasma stream motion. In all scenarios, the penetration of the melted material into the gaps is negligible, which is due to a rather small surface temperature at the lateral surface opposite to the plasma stream.

The final averaged shapes of erosion craters along the inclined top brush surfaces for different inclination angles β are demonstrated in Fig. 2 for the scenarios with the plasma impact angle $\alpha = 5°$. For the low β the melted material from the overheated lateral surface faced to the plasma stream is much more shifted to the centre of the top-brush surface in comparison with cases with effective gap shadowing, and the pronounced peaks up to 6 μm form in the roughness profile near the brush centers. For the case with effective gap shadowing, small peaks below 0.2 μm form at the edges of top-brush segments which are opposite to the plasma stream. For case with high inclination angle β the rather deep craters up to 1.5 μm may appear due to the rather intense evaporation of the overheated top-brush surface ($Q > 1.5$ MJ/m^2).

The simulation results demonstrate that for a given angle of the impacting stream the optimal inclination angle β exists. The dependence of the

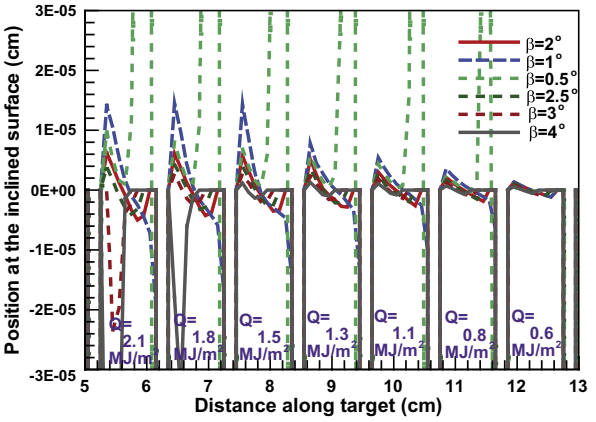

Fig. 2. Erosion profile along the inclined surface of the brushes for inclination angle β, $\alpha = 5°$.

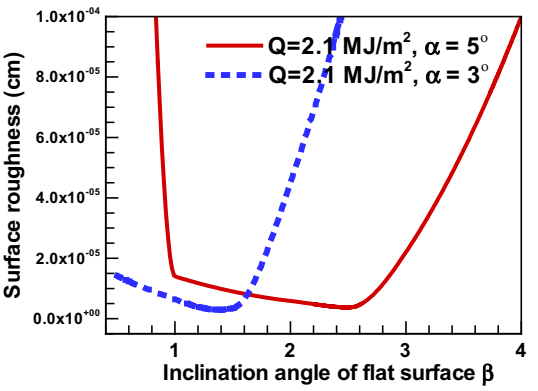

Fig. 3. Surface roughness versus the inclination angle β, for different inclination angle of damping plasma α.

surface roughness on the inclination angle β for two values of the plasma impact angle α is shown in Fig. 3. It can be seen, that the optimal angle β that gives a minimum of the surface roughness is practically half of the impacting angle α: $\beta_{opt} = 2.5°$ for the case with $\alpha = 5°$, and $\beta_{opt} = 1.5°$ for $\alpha = 3°$.

3. Simulation of the dome armour erosion damage of gaps

It is assumed that the heat flux profiles have a pronounced peak near the separatrix strike position (SSP); SSP stochastically changes along the divertor plate from one TE to another one having the Gaussian distribution with the dispersion ranging from 0.05 to 0.1 m.

Two scenarios are investigated: (1) short-time disruption with the SSP heat load $Q = 12$ MJ/m^2 and $\tau = 1$ ms and (2) long-time disruption with $Q = 30$ MJ/m^2 and $\tau = 10$ ms. The calculated radiation fluxes at the lateral walls of the dome for both scenarios are shown in Ref. [8].

The radiation transport in the plasma shield near the divertor surface is calculated using 45 groups of non-LTE Rosseland opacities for tungsten [10]. The absorption of the radiation heat load in the material vaporized from the dome surface is roughly taken into account, using the Bouguer low and the Rosseland opacities. For multiple TE, the total erosion is composed of the erosions of sequential TE with the stochastically varied SSP.

Simulations for the dome armour damage under radiation heat loads caused by single ELMs with $W \leqslant 4$ MJ/m^2 and $\tau = 0.2$–0.5 ms demonstrated that the temperature of W armour remains always below the melting point, which is due to a rather short irradiation time.

3.1. Erosion of dome armour

For both simulated scenarios the radiation fluxes at the dome surface reach 2–7 Gw/m^2 with the width of most irradiated area of 0.3–0.5 m, during several ms for the first scenario and more than 10 ms for the second one. The melt depth reaches 170–200 μm and the power at the dome surface is high enough for essential evaporation and formation of a rather thick 'secondary' shielding layer near the dome surface, with the plasma pressure of 1–2 bars. For both scenarios about 0.2–0.3 μm of W armour is evaporated after each disruption. The pressure gradient generates violent melt motion with the velocities below 0.6 m/s in both directions from the position of radiation flux maximum. After resolidification, the total magnitude of surface roughness is about 3 μm for the long-time disruption scenario. In case of short-time disruption the melt motion only weakly influences the total erosion profile: material loss about 0.3 μm caused mainly by the evaporation.

The simulation for the consequences of multiple disruptions implies the erosion additivity for multiple events. The plasma shield location and thus the position of radiation flux maximum changes in the same way as the SSP does. Fig. 4 demonstrates the maximum crater depth versus the number of disruptions for the Gaussian distribution of SSP with $\delta = 0.1$ m and 0.005 m. The total erosion of the dome surface after 10^2 disruptions is below 1 cm for the long-time and below 1 mm for the short-time disruptions. In assumption of stochastic motion of SSP the crater depth decreases by factor 1.5–2. Numerical simulation demonstrated that corresponding damages of the divertor plate are significantly less than it was obtained for the lateral dome surface: for example after 10^3 disruptions 2 mm and 0.3 mm, respectively.

3.2. Erosion of edge surface of W–Cu sandwich in gaps

The walls of the cassettes are designed as so called 'sandwiches' to be made of copper plates covered with either pure sintered W or tungsten lamellae [1]. Due to a geometric factor, the radiation fluxes impacting on the edge surfaces of the W–Cu sandwich inside the dome gaps are slightly less than the fluxes at the dome surface. Nevertheless, the radiation causes melting of W armour up to the depth of 100 μm and the melting of unprotected

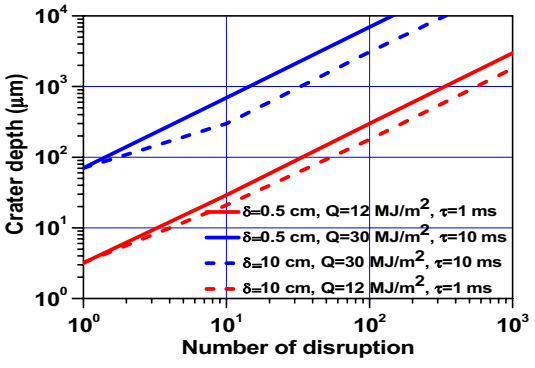

Fig. 4. Crater's maximum depth at the dome surface versus disruption number for $\delta = 0.5$ and $\delta = 10$.

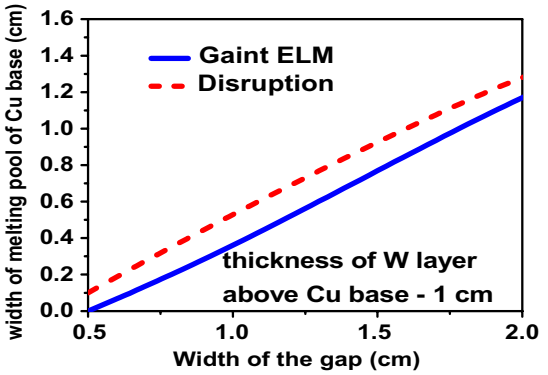

Fig. 5. Width of the melted Cu base versus the gap width between divertor cassettes.

Cu plate up to the depth of 200–300 μm [8] and its significant evaporation may occur. The secondary shielding layer formed near the edge surface, with the plasma pressure of several bars causes a violent melt motion along the gap surfaces with the velocities exceeding 1 m/s and thus to significant melt motion erosion of copper surface up to 30 μm (per one disruption), and the melt motion erosion of the edge nearby W of about 4 μm may occur.

The numerical simulations of erosion in the deep gaps between the divertor cassettes were carried out for the gap widths ranging from 0.2 cm up to 2 cm and W layer of 1 cm thickness. In case of ELMs and small gap width, the erosion in the deep gaps between the divertor cassettes is negligible for copper surface. Significant erosion may appear for the gap width between divertor cassettes exceeding 1 cm. The widths of the damaged copper versus gap width are shown in Fig. 5 for the disruption and Type I ELM. In case of disruptions the radiation from the plasma shielding causes melting of W armour up to the gap depth of 0.4 cm (the depth of melt pool is about 35 μm) and the melting of unprotected Cu plate up to the depth of several cm inside the gap with melt pool depth varying from 30 μm up to 100 μm in relation to the gap width. Melt motion produces a crater of the depth of 3 μm near the contact boundary between W and Cu.

For the multiple TE damage of the contact regions can linearly increases with number of transient events.

4. Conclusion

The modified MEMOS is applied for simulations of melt erosion of W-macrobrush armor caused by weak ELMs in ITER, aiming optimization of inclination of brushes top surfaces in order to provide efficient shadowing of brush edges faced to the impacting plasma stream. The shadowing prevents large overheating of the brush edges and significantly decreases surface roughness.

The numerical simulations demonstrated that an optimal inclination angle of brush surface can be found for each given inclination angle of the plasma stream and the other parameters of macrobrush elements.

Numerical simulations demonstrated that in case of disruptions a significant erosion of dome armour can be expected.

To prevent possible damage, all dome surfaces opened for the radiative heat load from the shielding layer in front of the divertor surface should be protected by tungsten armour.

It is worthwhile notify that the calculated load gives a lower estimation for the expected damage. The Rosseland opacities underestimate the radiation flux and comprehensive calculations can result in a factor up to 2 and in decreasing the energy threshold for dome damage.

Acknowledgements

This work, supported by the European Communities under the contract of Association between EURATOM and Forschungszentrum Karlsruhe, was carried out within the framework of the European Fusion Development Agreement. The views and opinions expressed herein do not necessarily reflect those of the European Commission.

References

[1] ITER Physics Basis, Nucl. Fusion 39 (1999).
[2] B. Bazylev, H. Wuerz, J. Nucl. Mater. 307–311 (2002) 69.
[3] H. Wuerz et al., J. Nucl. Mater. 307–311 (2002) 60.
[4] T.J. Renk et al., J. Nucl. Mater. 347 (2005) 266.
[5] A. Hassanein, I. Konkashbaev, J. Nucl. Mater. 290–293 (2001) 1074.
[6] B.N. Bazylev et al., J. Nucl. Mater. 337–339 (2005) 766.
[7] B.N. Bazylev et al., Fusion Eng. Des. 75–79 (2005) 407.
[8] B.N. Bazylev et al., Europhysics Conference Abstracts 29C, P-1.002.
[9] S.E. Pestchanyi, B.N. Bazylev, I.S. Landman, 31st EPS Conference on Plasma Physics, <http://eps2004.clf.rl.ac.uk/pdf/P1_135.pdf>.
[10] H. Wuerz et al., J. Nucl. Mater. 290–293 (2001) 1138.